

High-precision unambiguous tracking technique for BDS B1 wideband composite signal

Yang Gao^{1,2}  | Zheng Yao^{1,2}  | Mingquan Lu^{1,2}

¹ Department of Electronic Engineering, Tsinghua University, Beijing, China

² Beijing National Research Center for Information Science and Technology, Beijing, China

Correspondence

Zheng Yao, Department of Electronic Engineering, Tsinghua University, Beijing, China.

Email: yaozheng@tsinghua.edu.cn

Funding information

National Natural Science Foundation of China, Grant/Award Number: 61771272

Abstract

In the BeiDou Navigation Satellite System (BDS) B1 band, a single-sideband complex binary offset carrier (SCBOC) modulation is employed to combine the legacy and the modernized B1 signals into an asymmetric-wideband composite signal for the backward compatibility. However, SCBOC modulation has only been regarded as a means to achieve the co-existence between B1I and B1C signals, whose high-precision ranging potential is not fully understood or exploited. In this paper, a new pathway for BDS B1 receivers to further enhance their ranging precision is established for the first time, by proposing an unambiguous cross-assisted tracking (CAT) loop, which fully exploits the ranging performance of the SCBOC subcarrier and the inherent coherence between components in the composite signal. Simulation and experiment using live BDS-3 signals show that compared to the traditional tracking processing for independent components, the CAT loop can significantly improve ranging performance precision, thus providing a high-precision processing mode for the BDS B1 composite signal.

1 | INTRODUCTION

In recent years, with the rapid development of global navigation satellite systems (GNSS) and the continuous expansion of navigation applications, the number of new generation navigation signals has significantly increased, which not only makes the limited spectrum source more crowded but also makes the realization of signal multiplexing more difficult for satellite payloads. Additionally, the requirement for improving ranging and positioning performance is increasing. These constraints and demands have led to the long-term development of advanced signal structures and high-efficiency multiplexing technology. On the one hand, in the new generation GNSS signal structures, multiple subcarriers were introduced to not only achieve better spectrum separation but also to provide wider Gabor bandwidth as compared to a traditional binary phase shift keying (BPSK) modulated signal, thus yielding a high potential for improving ranging performance. Several examples include: the square-wave

subcarrier that was used in the simplest BOC modulation (Betz, 2001), the multilevel subcarrier that was chosen for the multiplexed BOC (MBOC) modulation (Hein et al., 2006), the double-sideband complex subcarrier that was applied to both the alternative BOC (AltBOC) modulation (Lestarquit, Artaud, & Issler, 2008) and the asymmetric constant envelope BOC (ACE-BOC) modulation (Yao, Zhang, & Lu, 2016), and the single-sideband complex subcarrier that was employed in the newest SCBOC modulation (Yao & Lu, 2013) in the BeiDou Navigation Satellite System (BDS) B1 band. On the other hand, the advanced constant envelope multiplexing (CEM) technology combines these complicated navigation signals components from the same satellite into a composite signal over a shared transmitting chain, which provides an opportunity for the combined reception and auxiliary processing between signal components (Zhou, Yao, & Lu, 2016).

Among these new generation GNSS signals, one of the most noteworthy signal structures is the combination of the civil signals B1I and B1C broadcast by the BDS-3 satel-

lites in the B1 band. The BDS requirement for backward compatibility makes the B1 band the first case to adopt single-sideband complex subcarrier and single-sideband multiplexing in the satellite navigation community. A unique multicarrier multiplexing technique, referred to as CEM via intermodulation construction (CEMIC) (Yao, Guo, Ma, & Lu, 2017; Yao & Lu 2017), is used to combine the legacy BII signal, the modernized B1C signal, and the authorized service B1A signal into an asymmetric-wideband composite signal. More specifically, the BII signal component of BDS-3 adopts SCBOC modulation to move its primary power from the BDS-3 B1 frequency (1575.42 MHz) to the legacy BDS-2 B1 frequency (1561.098 MHz) to meet the need for backward compatibility; therefore, it can be treated as a legacy BII narrowband signal by a conventional BDS-2 receiver. However, as of now, SCBOC modulation has only been regarded as a means to achieve the co-existence between BII and B1C signals and the smooth transition of the BDS. Its ranging accuracy potential is not yet fully understood or utilized.

It is not difficult to find that when the BDS-3 B1 frequency is chosen as the central frequency, the Gabor bandwidth of the BII signal will be greatly increased due to the single-sideband complex subcarrier of 14.322 MHz. Therefore, how to make full use of the potential advantages brought by the SCBOC modulation and composite signal structure to achieve performance improvement becomes an interesting problem to solve. However, there are several complicated difficulties and challenges in tracking signals with such modulation.

The first challenge is the well-known ambiguity threat. Similar to other split-spectrum signals such as BOC and MBOC modulated signals using real subcarriers, the complex subcarrier in SCBOC modulated signals introduces an ambiguity threat into the code-tracking process due to its multi-peak auto-correlation function (ACF). Side peak lock may occur, creating a bias in pseudorange measurements. The existing solutions of this issue are mainly divided into two categories: one-dimensional (1-D) tracking techniques that directly act on traditional one-dimensional correlation functions to achieve unambiguous operations (Fine & Fine, 1999; Ward, 2003; Julien, Macabiau, Cannon, & Lachapelle, 2007; Yao, Cui, Lu, & Feng, 2010), and two-dimensional (2-D) tracking techniques that solve the ambiguity problem by adding an additional subcarrier loop to independently track the subcarrier-dimensional phase delay and transform the signal correlation function into a two-dimensional space (Hodgart, Blunt, & Unwin, 2007; Borio, 2014, 2017; Tian, Zhang, & Cheng, 2016; Schubert, Wendel, Soellner, Kaindl, & Kohl, 2014). In these existing methods, compared to 1-D tracking techniques, the 2-D loop structures are more general and usually considered to be more promising for

their better performance, as has been verified by several parties (Lohan et al., 2017; Yao, Gao, Gao, & Lu, 2017; Gao, Yao, & Lu, 2018). However, all of the existing unambiguous tracking methods can only be used for cases where the signal correlation function is a real function, and thus are not suitable for SCBOC modulated signal tracking.

In addition to the multi-peak ambiguity problem, the single-sideband complex subcarrier also presents the challenge of the complex ACF, which means there exists a serious coupling relation between the phase-estimation error of the subcarrier and that of the carrier (Sleewaegen, De Wilde, & Hollreiser, 2004). Such a complex correlation function cannot be simply tracked since the estimation errors of the subcarrier and the carrier are not clearly separated. This means any subcarrier phase-estimation error will result in the tracking deviation of the carrier phase and vice versa. Therefore, there are very few existing tracking methods for SCBOC modulated signals. One possible solution referred to as BPSK-like is to treat the subcarrier estimation error as the carrier tracking deviation, although this means the ranging performance improvement brought by the subcarrier is lost (Martin, Leblond, Guillotel, & Heiries, 2003). Obviously, such a narrowband receiving mode pays a great price in ranging performance in exchange for stable tracking. Another possible method is to jointly process two complex conjugate SCBOC modulated signals, such as AltBOC or ACE-BOC, in which the nonzero imaginary part of the correlation function is removed and only the real part is retained (Zhu, Cui, & Lu, 2015; Ren, Jia, Chen, & Yao, 2012). Therefore, none of these methods can be used for single-sideband SCBOC modulated signals.

These difficulties and challenges have seriously hindered the utilization of the high-precision ranging advantages brought by SCBOC. To solve these problems, this paper, for the first time, proposes a processing mode that makes full use of the structural characteristics of the B1 wideband composite signal, which can be used to achieve high-precision ranging and positioning. More specifically, an unambiguous cross-assisted tracking (CAT) loop based on 2-D loops for BDS B1 wideband composite signal is proposed. The CAT loop makes full use of the inherent coherence between the components in the B1 wideband composite signal, and not only overcomes the ambiguity threat but also solves the coupling challenge, while fully exploiting the high-precision ranging performance brought by the high-frequency SCBOC subcarrier.

The main contributions of this paper include three aspects: first, the concept of utilizing the B1 SCBOC subcarrier in the receiver for high-precision ranging is proposed for the first time, which establishes a new way for BDS B1 receivers to further enhance their ranging accuracy. Second, a specific implementation method of

TABLE 1 BDS-3 signal structure in the B1 band

Signal	Component	Carrier Frequency/MHz	Code Rate/Mcps	Subcarrier Frequency/MHz	Modulation	Service Type	System
B1I*	–	1561.098	2.046	–	BPSK(2)	Open	BDS-2
B1I	–	1575.42	2.046	14.322	SCBOC(14,2)	Open	BDS-3
B1C	Pilot	1575.42	1.023	1.023/6.138	QMBOC(6,1,4/33)	Open	BDS-3
	Data	1575.42	1.023	1.023	BOC(1,1)	Open	BDS-3
B1A		1575.42		Undocument		Authorized	BDS-3

SCBOC signal high-precision tracking, the unambiguous CAT loop, is proposed in which the inherent coherence between the components in the composite signal is used to solve the problem that the complex correlation function cannot be tracked. Furthermore, a 2-D loop structure is used to transform the signal correlation function into a 2-D space to solve the tracking ambiguity threat. In addition to establishing a standard tracking loop architecture, several optional optimization schemes are also provided that can enhance receiver operation. Third, the correctness and effectiveness of the proposed algorithm are verified by the results of simulated signal analysis as well as real BDS-3 signal processing. The results show that compared to the traditional tracking processing for independent components, the proposed CAT technique for the composite signal can significantly improve ranging precision. The CAT technique pioneers a high-precision processing mode for the BDS-3 B1 composite signal, which can provide significant reference and guidance for the high-precision utilization of the new generation BDS signal.

The remainder of the paper is organized as follows. Section 2 reviews the structure of the BDS B1 composite signal. Then, the characteristics of the SCBOC modulated signal are analyzed, and its tracking challenges are presented in Section 3. The proposed unambiguous CAT loop for the B1 composite signal is illustrated in detail in Section 4. The results of simulation and real data experiments are provided in Section 5. Finally, conclusions and future work are discussed in Section 6.

2 | BDS B1 WIDEBAND COMPOSITE SIGNAL

According to the development plan of BDS-3, in addition to broadcasting the new modernized B1C signal and the authorized service B1A signal, the Medium Earth Orbit (MEO) and Inclined Geosynchronous Satellite Orbit (IGSO) satellites of BDS-3 need to be backward compatible with the legacy BDS-2 B1I signal. Although these signals are all in the B1 band, their central frequencies are different. The nominal carrier frequency of the legacy B1I signal in BDS-2 is $f_{B1I} = 1561.098$ MHz, while the cen-

tral frequency of the B1 signal in BDS-3 is $f_{B1} = 1575.42$ MHz. Therefore, in order to meet the constraints of a smooth evolutionary transition and backward compatibility of the BDS, SCBOC modulation and CEMIC technique are adopted in the B1 band for BDS-3. The legacy B1I signal, the modernized B1C signal, and the authorized service B1A signal are combined into an asymmetric, wideband composite signal with the central frequency at 1575.42 MHz.

Table 1 shows the BDS-3 signal structure in the B1 band. The SCBOC(14,2) modulation is used for backward compatibility with legacy B1I signal, and quadrature multiplexed BOC (QMBOC) modulation is applied in the modernized B1C signal to achieve compatibility and interoperability with the GPS and Galileo systems.

Therefore, the BDS-3 B1 wideband radio frequency (RF) composite signal can be modeled as:

$$S_{B1}(t) = \operatorname{Re} \left\{ \left(\sqrt{P_{B1I}} e^{j\phi_{B1I}} s_{B1I}(t) + \sqrt{P_{B1C}} e^{j\phi_{B1C}} s_{B1C}(t) \right) \right. \\ \left. + \sqrt{P_{B1A}} e^{j\phi_{B1A}} s_{B1A}(t) + I_{IM}(t) \right\} e^{j2\pi f_{B1} t}, \quad (1)$$

where P_i , ϕ_i , and $s_i(t)$ are the nominal power, initial phase, and baseband complex envelope of the corresponding signal component $i = B1I, B1C, B1A$, respectively. The initial phases ϕ_{B1I} and ϕ_{B1C} are equal, and the baseband complex envelope can be further given by

$$s_{B1I}(t) = d_{B1I}(t) c_{B1I}(t) \gamma_{sc}(t) \quad (2)$$

$$s_{B1C}(t) = \frac{1}{2} d_{B1C}(t) c_{B1C-d}(t) sc_a(t) \\ + c_{B1C-p}(t) \left[\sqrt{\frac{1}{11}} sc_b(t) + j \cdot \sqrt{\frac{29}{44}} sc_a(t) \right], \quad (3)$$

where $d_{B1I}(t)$ and $d_{B1C}(t)$ are the navigation messages of the B1I and B1C signal, respectively. $c_{B1I}(t)$, $c_{B1C-d}(t)$, and $c_{B1C-p}(t)$ are the ranging codes of the B1I signal, data channel, and pilot channel of the B1C signal, respectively. $sc_a(t) = \operatorname{sgn}(\sin(2\pi f_{sc,a} t))$ and $sc_b(t) = \operatorname{sgn}(\sin(2\pi f_{sc,b} t))$ are the sine-phased square-wave subcarriers with subcarrier frequency $f_{sc,a} = 1f_0$ and $f_{sc,b} = 6f_0$ used by the

narrowband BOC(1,1) component and the wideband BOC(6,1) component, respectively, where $f_0 = 1.023$ MHz is the GNSS baseline frequency.

$$\gamma_{sc}(t) = \text{sgn}(\cos(2\pi f_{sc,B1I} t)) - j \cdot \text{sgn}(\sin(2\pi f_{sc,B1I} t)) \quad (4)$$

is the single-sideband complex subcarrier with the frequency of $f_{sc,B1I} = f_{B1} - f_{B1I} = 14f_0$, where $\text{sgn}(x)$ is the sign function which takes the value of 1 for $x \geq 0$ and -1 for $x < 0$. $I_{IM}(t)$ is the additional intermodulation term to maintain the constancy of the composite signal envelope (Yao et al., 2017; Yao & Lu, 2017).

The transparency constraint of the CEMIC technique ensures that each signal component can be received separately and the influence of the B1A signal and the intermodulation term on the open-service signal component

where τ is the signal propagation delay, f_D is the Doppler shift, φ is the carrier phase, and $n(t)$ is the zero-mean Gaussian white noise with PSD N_0 .

Signal (5) is first bandlimiting filtered and then down-converted by the receiver front end. Since the subcarrier frequency of the SCBOC(14,2) modulated signal is much higher than that of the B1C pilot BOC(1,1) modulated signal, the influence of the bandlimiting filter on the former is much more serious than on the latter, which means the bandlimiting effect on the SCBOC(14,2) modulated signal cannot be ignored. More specifically, the high-frequency signal components of the SCBOC are removed and only the lowest order term is preserved, which means Equation (4) can be approximated as $\gamma_{sc}(t) \approx e^{-j2\pi f_{sc,B1I} t}$. This approximation will be justified and can be verified from the spectrum analysis of the SCBOC(14,2) modulated signal in the next section. Therefore, the bandlimiting filtered B1I signal can be represented as

$$\begin{aligned} \tilde{r}_{B1I}(t) &\approx \sqrt{P_{B1I}} d_{B1I}(t - \tau) c_{B1I}(t - \tau) \left[\cos(2\pi f_{sc,B1I}(t - \tau)) \cos(2\pi(f_{B1} + f_D)t + \varphi) \right. \\ &\quad \left. + \sin(2\pi f_{sc,B1I}(t - \tau)) \sin(2\pi(f_{B1} + f_D)t + \varphi) \right] \\ &= \sqrt{P_{B1I}} d_{B1I}(t - \tau) c_{B1I}(t - \tau) \cos(2\pi(f_{B1} - f_{sc,B1I} + f_D)t + \varphi + 2\pi f_{sc,B1I}\tau). \end{aligned} \quad (6)$$

receiving can be assumed to be negligible. Therefore, only open-service signals need to be considered. Additionally, it should be noted that these signal components are combined into a digital-baseband composite signal and they share a common transmitting chain impacted by the same environment. Therefore, the strictly determined amplitude and phase relationship between the signal components is maintained from the payload of the satellite to the antenna of the receiver. Using Equations (1)-(4), the received B1 wideband composite signal (open part) at the antenna of the GNSS receiver can be represented as

$$\begin{aligned} r_{B1}(t) &= \underbrace{\sqrt{P_{B1I}} d_{B1I}(t - \tau) c_{B1I}(t - \tau) \left[\text{sgn}(\cos(2\pi f_{sc,B1I}(t - \tau))) \cos(2\pi(f_{B1} + f_D)t + \varphi) \right.} \\ &\quad \left. + \text{sgn}(\sin(2\pi f_{sc,B1I}(t - \tau))) \sin(2\pi(f_{B1} + f_D)t + \varphi) \right]}_{r_{B1I}(t)} \\ &+ \underbrace{\frac{1}{2} \sqrt{P_{B1C}} d_{B1C}(t - \tau) c_{B1C-d}(t - \tau) s_{c_a}(t - \tau) \cos(2\pi(f_{B1} + f_D)t + \varphi)}_{r_{B1C-d}(t)} \\ &+ \underbrace{\sqrt{\frac{P_{B1C}}{11}} c_{B1C-p}(t - \tau) s_{c_b}(t - \tau) \cos(2\pi(f_{B1} + f_D)t + \varphi)}_{r_{B1C-pb}(t)} \\ &- \underbrace{\sqrt{\frac{29P_{B1C}}{44}} c_{B1C-p}(t - \tau) s_{c_a}(t - \tau) \sin(2\pi(f_{B1} + f_D)t + \varphi) + n(t)}_{r_{B1C-pa}(t)}, \end{aligned} \quad (5)$$

It can be seen from Equation (6) that the BDS-3 BII signal using SCBOC(14,2) modulation can be easily processed by the traditional BDS-2 receiver as a legacy BPSK(2) modulated signal, which meets the requirement of backward compatibility. However, as of now, SCBOC modulation has only been regarded as a means to achieve the multifrequency multiplexing of the B1 signal and the smooth evolutionary transition of the BDS. The performance potential of SCBOC in the pseudorange measurement brought by the subcarrier is not yet fully realized and utilized. Although the BPSK-like receiving mode is capable of processing a

BII signal, the ranging performance provided by the single-sideband complex subcarrier is lost. It would be a significant performance loss if such a huge potential in ranging and positioning performance cannot be used. To solve this problem, the characteristics of the SCBOC(14,2) modulated signal, the difficulties and challenges in wideband receiving mode should first be fully analyzed and understood.

3 | TRACKING OF THE SCBOC MODULATED SIGNAL

This section is mainly divided into two parts. The first part analyzes the tracking-performance potential of the SCBOC(14,2) modulated signal from the perspective of power spectral density (PSD) and Gabor bandwidth. The second part shows the difficulties and challenges in the wideband receiving mode from the perspective of tracking loops and ACF.

3.1 | Characteristics of the SCBOC modulated signal

The PSD of the baseband complex envelope of the SCBOC(14,2) modulated signal is represented as

$$S_{BII}(f) = \frac{16 \left(1 + 2 \cos\left(\frac{2\pi f T_c}{7}\right) + 2 \cos\left(\frac{4\pi f T_c}{7}\right) + 2 \cos\left(\frac{6\pi f T_c}{7}\right) \right)^2 \sin^4\left(\frac{\pi f T_c}{28}\right) \left(1 + \cos\left(\frac{\pi f T_c}{14}\right) - \sin\left(\frac{\pi f T_c}{14}\right) \right)^2}{\pi^2 f^2 T_c}, \quad (7)$$

where $T_c = \frac{1}{f_c}$ is the width of the ranging code and f_c is the code rate. The specific derivation process is shown in the Appendix.

Figure 1 shows the PSD of SCBOC(14,2) modulated signals with different receiver front-end bandwidths. As can be seen from Figure 1, the PSD of the SCBOC(14,2) modulated signal is asymmetric about the central frequency, which is different from BPSK and BOC modulated signals. The reason for this special phenomenon is that the main harmonic component of the single-sideband complex subcarrier shown in Equation (4) is concentrated at $-f_{sc,BII}$, while no harmonic component exists at $f_{sc,BII}$. Therefore, the first main lobe of the SCBOC(14,2) modulated signal is moved to the lower sideband away from the central frequency of $f_{sc,BII}$, showing the asymmetric PSD. It is not difficult to verify that in order to contain the first main lobe of the SCBOC(14,2) modulated signal, the front-end bandwidth should be no less than 32.736 MHz. In addition, when the front-end bandwidth is greater than 90.024 MHz, the energy of the second side lobe is

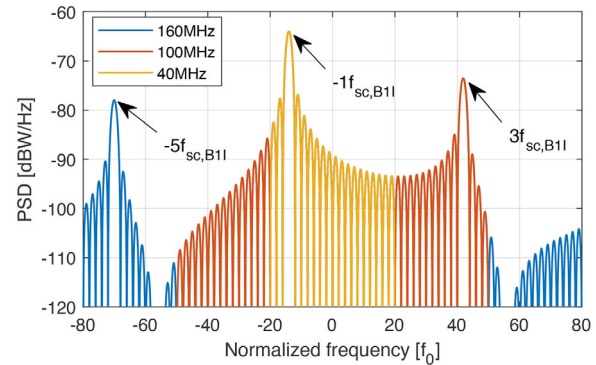


FIGURE 1 Power spectral density of SCBOC(14,2) modulated signal with different front-end bandwidths [Color figure can be viewed in the online issue, which is available at wileyonlinelibrary.com and www.ion.org]

preserved. Therefore, when the receiver front-end bandwidth is in the range of 32.736 MHz to 90.024 MHz, all the high-frequency components of the square-wave subcarrier will be removed, and only the first-order term will be preserved. Considering that the front-end bandwidth of most GNSS receivers is much less than 90 MHz, the approximation $\gamma_{sc}(t) \approx e^{-j2\pi f_{sc,BII} t}$ in the previous section is justified.

Figure 2 shows the comparison of normalized PSD between BDS-2 BII BPSK(2) and BDS-3 BII SCBOC(14,2) modulated signals when the front-end bandwidth is 40

MHz. The value 0 on the x-axis represents the center frequency of the BDS-3 B1 band, which is 1575.42 MHz.

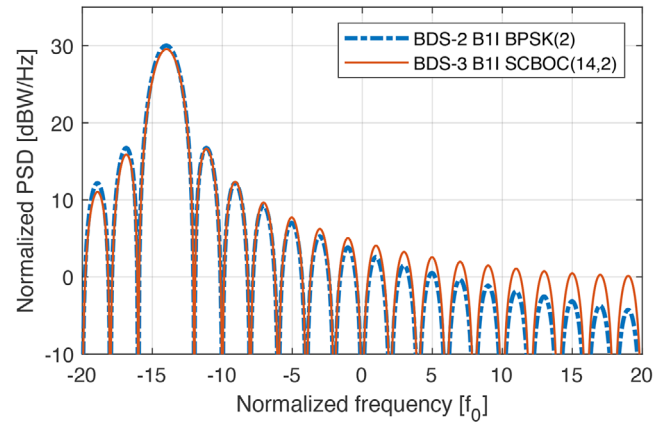


FIGURE 2 Comparison of normalized power spectral density between BDS-2 BII BPSK(2) and BDS-3 BII SCBOC(14,2) modulated signals [Color figure can be viewed in the online issue, which is available at wileyonlinelibrary.com and www.ion.org]

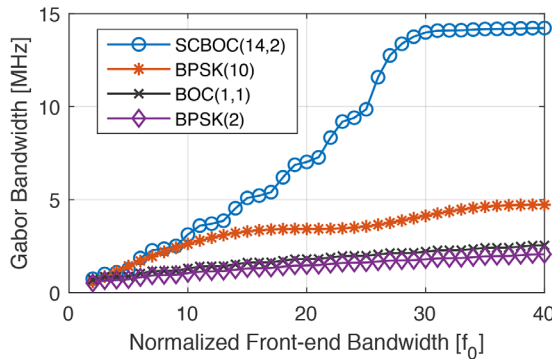


FIGURE 3 Comparison between the SCBOC(14,2) modulated signal and several other signals in terms of the Gabor bandwidth [Color figure can be viewed in the online issue, which is available at wileyonlinelibrary.com and www.ion.org]

Note that the center frequency of the BDS-2 B1I BPSK(2) modulated signal is 1561.098MHz, which is 14.322MHz away from the BDS-3 B1 frequency. It can be seen from Figure 2 that the spectrum of the two modulated signals is very similar, which means the BDS-3 SCBOC(14,2) modulated signal can be treated as a legacy BPSK(2) modulated signal to achieve the smooth evolutionary transition of BDS. However, there are some differences in the spectrum of the two signals. The farther away from the first main lobe, the more obvious the difference between the two signals.

Based on the PSD, the signal Gabor bandwidth, which is an important indicator used to evaluate the theoretical limit of the signal thermal noise performance, can be calculated by

$$\text{GaborBW} = \sqrt{\frac{\int_{-\frac{\beta_r}{2}}^{\frac{\beta_r}{2}} f^2 S(f) df}{\int_{-\frac{\beta_r}{2}}^{\frac{\beta_r}{2}} S(f) df}}, \quad (8)$$

where β_r is the receiver front-end bandwidth and $S(f)$ is the normalized PSD. Generally, the wider the Gabor bandwidth, the better the thermal noise performance, which means the potential of signal in ranging and positioning performance is greater.

Figure 3 shows the Gabor bandwidth of the SCBOC(14,2) modulated signal. The results for BOC(1,1), BPSK(2), and BPSK(10) modulated signals are also given as a comparison. It can be seen from Figure 3 that when the front-end bandwidth is greater than 6 MHz, the SCBOC(14,2) modulated signal has the widest Gabor bandwidth, especially when the front-end bandwidth is wide enough to contain its main lobe. For example, when the front-end bandwidth is $30f_0$, which means the whole main lobe of the SCBOC(14,2) modulated signal can be contained,

the Gabor bandwidth of the SCBOC(14,2) modulated signal is about eight times the Gabor bandwidth of BPSK(2), six times the Gabor bandwidth of BOC(1,1), and three times the Gabor bandwidth of BPSK(10) modulated signals, respectively. Therefore, the SCBOC(14,2) modulated signal has a huge potential for increased ranging performance, but this requires addressing multiple implementation difficulties and challenges first.

3.2 | Challenges in matched tracking for the SCBOC modulated signal

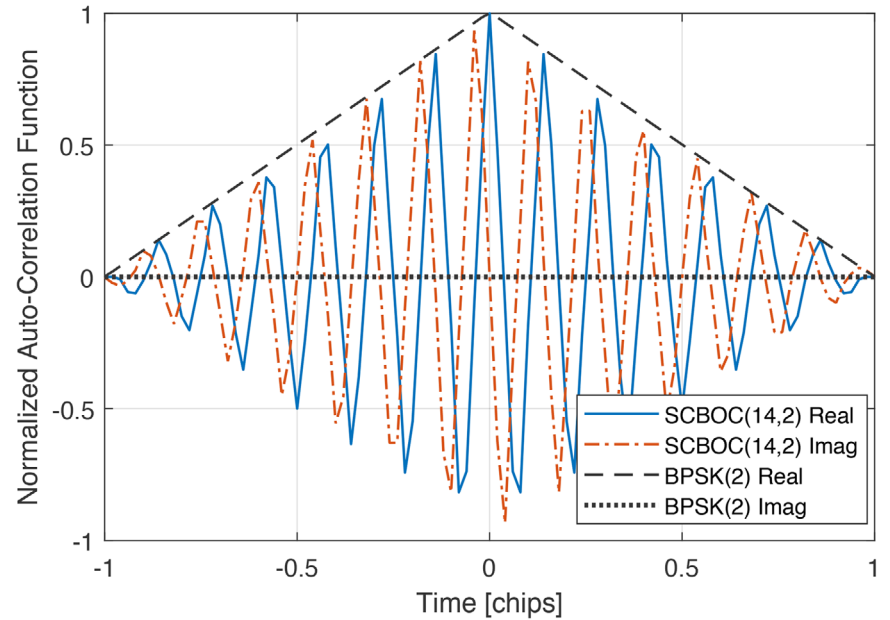
In stable tracking loops, the received signal is first multiplied by the locally generated replica carrier and code, then coherent integration is used to obtain the correlation results, which are sent to the discriminators and filters of the feedback loop to update the corresponding estimation value and keep the stable tracking state. Therefore, we first assume that the SCBOC(14,2) modulated signal in matched receiving mode is well-tracked and then analyze the factors that affect the tracking loops to keep them stable. The prompt correlation results are given by

$$\begin{aligned} I_{B1I,P} &= \frac{1}{T} \int_0^T r_{B1I}(t) \cdot \cos(2\pi(f_{B1} - f_{sc,B1I} + \hat{f}_D)t \\ &\quad + \hat{\phi} + 2\pi f_{sc,B1I}\hat{\tau}) \cdot c_{B1I}(t - \hat{\tau}) \cdot dt \\ &\approx d\sqrt{2P_{B1I}}R_{B1I}(\Delta\tau)\text{sinc}(\Delta f_D T) \\ &\quad \times \cos(\pi\Delta f_D T + \Delta\varphi + 2\pi f_{sc,B1I}\Delta\tau) \\ Q_{B1I,P} &= \frac{1}{T} \int_0^T r_{B1I}(t) \cdot \sin(2\pi(f_{B1} - f_{sc,B1I} + \hat{f}_D)t \\ &\quad + \hat{\phi} + 2\pi f_{sc,B1I}\hat{\tau}) \cdot c_{B1I}(t - \hat{\tau}) \cdot dt \\ &\approx d\sqrt{2P_{B1I}}R_{B1I}(\Delta\tau)\text{sinc}(\Delta f_D T) \\ &\quad \times \sin(\pi\Delta f_D T + \Delta\varphi + 2\pi f_{sc,B1I}\Delta\tau), \end{aligned} \quad (9)$$

where T is the coherent integration time; \hat{f}_D , $\hat{\phi}$, and $\hat{\tau}$ are the estimations of Doppler shift, carrier phase, and propagation delay, respectively; $\Delta f_D = f_D - \hat{f}_D$, $\Delta\varphi = \varphi - \hat{\phi}$, and $\Delta\tau = \tau - \hat{\tau}$ are the corresponding estimation errors, respectively; d is the navigation message, which is assumed to take a constant value over the coherent integration period; $R_{B1I}(\Delta\tau)$ is the ACF of the BPSK(2) modulated signal; and $\text{sinc}(x) \triangleq \frac{\sin(\pi x)}{\pi x}$ is the normalized sinc function.

Figure 4 shows the real part $I_{B1I,P}$ and imaginary part $Q_{B1I,P}$ of the ACF of the SCBOC(14,2) modulated signal when $\Delta f_D = 0$ and $\Delta\varphi = 0$. In contrast, the ACF of the BPSK(2) modulated signal is also given. It can be seen from Figure 4 that the ACF of the SCBOC (14, 2)

FIGURE 4 ACF of the SCBOC(14,2) modulated signal [Color figure can be viewed in the online issue, which is available at wileyonlinelibrary.com and www.ion.org]



modulated signal has multiple peaks, which is similar to other split-spectrum signals. Compared with the ACF of the BPSK(2) modulated signal, the ACF of the SCBOC(14,2) modulated signal has a much sharper main peak, which means higher ranging performance. However, since the ACF of the SCBOC(14,2) modulated signal has many side peaks, stable tracking of the main peak instead of the side peaks is very difficult. Therefore, a serious ambiguity threat is an important factor affecting the stable tracking of the SCBOC(14,2) modulated signals in matched receiving mode.

In addition to the multi-peak ambiguity problem, it can be seen from Equation (9) and Figure 4 that the ACF of the SCBOC(14,2) modulated signal is a complex function, which is different from the previous GNSS signals. More specifically, the propagation delay estimation error $\Delta\tau$ not only exists in the code dimension correlation function R_{B1I} , but also coexists with $\Delta\phi$ in the subsequent trigonometric function. Although $\Delta\tau$ in the code dimension correlation function can be stably tracked, it only has a low-precision ranging performance equivalent to a BPSK(2) modulated signal. Therefore, in order to utilize the ranging performance brought by the high-frequency subcarrier, the $\Delta\tau$ in the trigonometric function should be estimated. However, due to the existence of the coupling relation between $\Delta\tau$ and $\Delta\phi$, such a complex correlation function cannot be tracked in a conventional receiver since the estimation errors of the subcarrier and carrier are not clearly separated. This means any subcarrier phase-estimation error will result in the tracking deviation of the carrier phase and vice versa. Therefore, the challenge that the complex correlation function cannot be well-tracked is the other important factor affecting the stable tracking of

the SCBOC(14,2) modulated signal in the matched receiving mode.

These difficulties and challenges have seriously hindered the utilization of the high-precision ranging advantages brought by SCBOC.

4 | UNAMBIGUOUS CROSS-ASSISTED TRACKING METHOD

This section makes full use of the coherence and the structural characteristics of the B1 wideband composite signal and aims not only to overcome the ambiguity threat but also to solve the coupling challenge, while fully exploiting the high-precision ranging performance brought by the high-frequency subcarrier. More specifically, an unambiguous cross-assisted tracking method based on two-dimensional loops is proposed.

Since the strictly determined amplitude and phase relationship between the signal components in the B1 composite signal is maintained from the satellite payload to the receiver antenna, the inherent coherence between the signal components can be used to solve the problem that the complex correlation function cannot be tracked. More specifically, the carrier estimate of the composite signal can be obtained by the B1C component, which is stable and insensitive to the propagation delay estimation error. Considering the coherence between the B1I and B1C components in BDS-3, the carrier estimation of the B1I component can be recovered from that of the B1C component. When the carrier of the SCBOC(14,2) modulated signal is well-tracked, the strong coupling relation between the estimation errors of subcarrier and carrier can be effectively

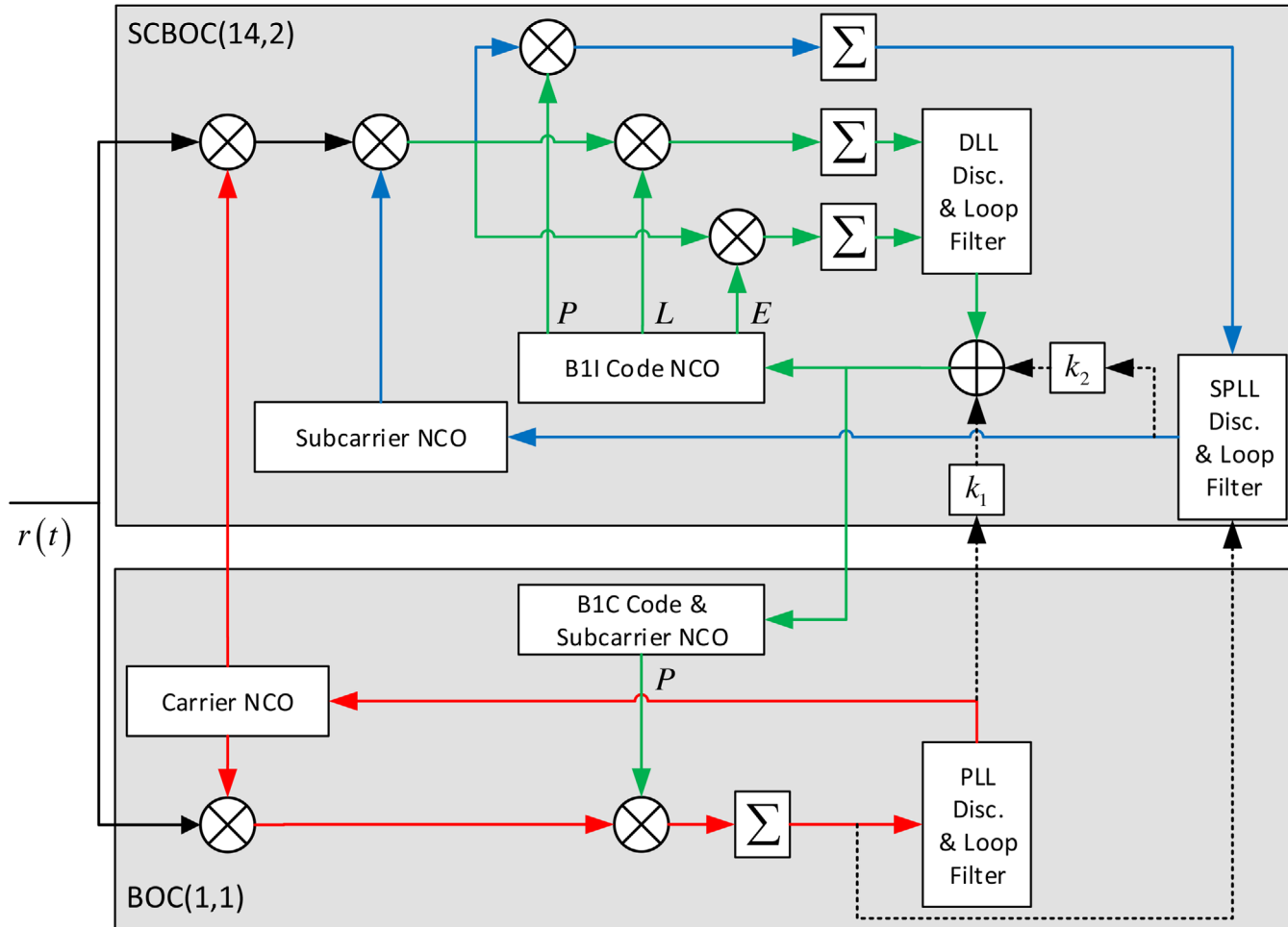


FIGURE 5 Schematic representation of the cross-assisted tracking loops for B1 composite signal, carrier loop (red), code loop (green), subcarrier loop (blue), optional optimization (dotted line) [Color figure can be viewed in the online issue, which is available at wileyonlinelibrary.com and www.ion.org]

separated, which means the complex correlation peak can be tracked.

In addition to the coupling challenge, a serious ambiguity threat exists in the correlation function of the SCBOC(14,2) modulated signal. A 2-D tracking loop can be used to transform the signal correlation function into a 2-D space to solve the tracking ambiguity threat. More specifically, an unambiguous but low-precision phase delay estimation in the code dimension can be tracked by a conventional delay lock loop (DLL), and a high-precision but ambiguous phase delay estimation in the subcarrier dimension can be obtained by an additional subcarrier phase lock loop (SPLL). Then, the two phase delay estimations can be recombined to develop the unambiguous and high-precision propagation delay estimation. Considering the coherence between the B1I and B1C components in BDS-3, the propagation delay estimation of the B1C component can be recovered from that of the B1I component.

Figure 5 shows the schematic representation of the cross-assisted tracking loops for the B1 wideband compos-

ite signal. Colors help identify different loops. The carrier loop is in red, the code loop is in green, and the subcarrier loop is in blue. The dotted lines represent the optional optimization schemes, including the carrier-aided code technique, subcarrier-aided code technique, and noncoherent processing technique. For the sake of simplicity, all signals in Figure 5 are complex signals.

It should be noted that in a CAT loop, only a standard phase lock loop (PLL) is needed to track the Doppler shift and carrier phase of the composite signal since the signal components share a common carrier. More detailed, PLL uses prompt code and subcarrier of the B1C pilot BOC(1,1) component to track the carrier of the B1 composite signal. Similarly, only a standard DLL is necessary to estimate the code dimension phase delay since the ranging codes between the signal components are always strictly aligned. More detailed, DLL uses early and late code of the B1I signal to obtain an unambiguous but low-precision code dimension phase delay estimation, which is good enough to recover the code and subcarrier of the B1C pilot

BOC(1,1) component and the code of B1I component. In addition, an SPLL is introduced to estimate the single-sideband complex subcarrier. Similar to other 2-D tracking techniques (Hodgart et al., 2007; Borio, 2014, 2017; Tian et al., 2016; Schubert et al., 2014), a high-precision but ambiguous phase delay estimation in the subcarrier dimension can be obtained by SPLL. Finally, the two phase delay estimations from DLL and SPLL can be recombined to obtain the unambiguous and high-precision propagation delay estimation.

At first, the carrier of the BOC(1,1) and the SCBOC(14,2) modulated signal can be removed from the received B1 composite signal by multiplying locally generated complex carriers $y_{B1C}(t) = e^{-j(2\pi(f_{B1} + \hat{f}_D)t + \phi + \frac{\pi}{2})}$ and $y_{SCBOC}(t) = e^{-j(2\pi(f_{B1} + \hat{f}_D)t + \phi)}$, generated from the same PLL, where $\frac{\pi}{2}$ represents the two signal components that are phase-orthogonal.

Then, after removing the carrier, the subcarrier of the received SCBOC(14,2) modulated signal can be removed by multiplying the complex conjugate of the subcarrier exponential, i.e., $\hat{y}(t) = e^{j(2\pi\hat{f}_{sc,B1I}t - \hat{\phi}_{sc,B1I})}$, where $\hat{f}_{sc,B1I}$ is the estimation of the subcarrier frequency, and $\hat{\phi}_{sc,B1I} = 2\pi\hat{f}_{sc,B1I}\hat{\tau}_s$ is the estimation of the subcarrier phase, which is used to align the subcarrier phase between the received signal and the locally generated signal, where $\hat{\tau}_s$ is the phase delay estimation in the subcarrier dimension.

Finally, the product of the locally generated code with the received SCBOC(14,2) modulated signal is subjected to the coherent integration to calculate the early (E), prompt (P), and late (L) correlation results

$$R_{i-SCBOC} = \frac{1}{T} \int_0^T r_{B1}(t) \cdot y_{SCBOC}(t) \cdot \hat{y}(t) \cdot c_{B1I}(t - \hat{\tau}_c + \tau'_i) \cdot dt, \quad (10)$$

where $\hat{\tau}_c$ is the phase delay estimation in code dimension and the subscript $i \in \{E, P, L\}$ stands for the branches of E, P, and L, with the additional phase delays of $\tau'_E = -\Delta_c/2$, $\tau'_P = 0$, and $\tau'_L = \Delta_c/2$, respectively, in which Δ_c is the spacing between E and L replicas for the code discriminator and it is assumed to be in the range $0 \leq \Delta_c \leq T_c$.

Similarly, the product of the locally generated prompt code and subcarrier with the received BOC(1,1) modulated signal is subjected to the coherent integration to calculate the P correlation results, which are given by

$$R_{P-B1C} = \frac{1}{T} \int_0^T r_{B1}(t) \cdot y_{B1C}(t) \cdot C_{B1C_pilot}(t - \hat{\tau}_c) \times sign(\sin(2\pi f_{sc,B1C_a}(t - \hat{\tau}_c))) \cdot dt. \quad (11)$$

Therefore, it is not difficult to calculate the correlator results, which can be expressed as

$$\begin{aligned} I_{B1C,P} &= \sqrt{2P_{B1C}} R_{B1C} (\tau - \hat{\tau}_c) \text{sinc}(\Delta f_D T) \\ &\quad \times \cos(\pi \Delta f_D T + \Delta \varphi) \\ Q_{B1C,P} &= \sqrt{2P_{B1C}} R_{B1C} (\tau - \hat{\tau}_c) \text{sinc}(\Delta f_D T) \\ &\quad \times \sin(\pi \Delta f_D T + \Delta \varphi) \\ I_{SCBOC,i} &= d \sqrt{2P_{B1I}} R_{B1I} (\tau - \hat{\tau}_c + \tau'_i) \\ &\quad \times \text{sinc}((\Delta f_D - \Delta f_{sc,B1I}) T) \\ &\quad \times \cos(\pi(\Delta f_D - \Delta f_{sc,B1I}) T + \Delta \varphi + \Delta \varphi_{sc,B1I}) \\ Q_{SCBOC,i} &= d \sqrt{2P_{B1I}} R_{B1I} (\tau - \hat{\tau}_c + \tau') \\ &\quad \times \text{sinc}((\Delta f_D - \Delta f_{sc,B1I}) T) \\ &\quad \times \sin(\pi(\Delta f_D - \Delta f_{sc,B1I}) T + \Delta \varphi + \Delta \varphi_{sc,B1I}), \end{aligned} \quad (12)$$

where $i \in \{E, P, L\}$, $R_{B1C}(\tau)$ is the ACF of BOC(1,1) modulated signal, $R_{B1I}(\tau)$ is the code dimension ACF of the SCBOC(14,2) modulated signal, $\Delta f_{sc,B1I} = f_{sc,B1I} - \hat{f}_{sc,B1I}$ is the subcarrier frequency estimation error, and

$$\Delta \varphi_{sc,B1I} = 2\pi(f_{sc,B1I}\tau - \hat{f}_{sc,B1I}\hat{\tau}_s) \quad (13)$$

is the subcarrier phase-estimation error. It should be noted that the noise terms are ignored in the correlation results just for the sake of simplicity.

By assuming the perfect Doppler shift and subcarrier frequency synchronization, that is, $\Delta f_D \approx 0$ and $\Delta f_{sc,B1I} \approx 0$, the correlator results in Equation (12) can be further simplified as

$$\begin{aligned} I_{B1C,P} &= \sqrt{2P_{B1C}} R_{B1C} (\tau - \hat{\tau}_c) \cos(\Delta \varphi) \\ Q_{B1C,P} &= \sqrt{2P_{B1C}} R_{B1C} (\tau - \hat{\tau}_c) \sin(\Delta \varphi) \\ I_{SCBOC,i} &= d \sqrt{2P_{B1I}} R_{B1I} (\tau - \hat{\tau}_c + \tau'_i) \cos(\Delta \varphi + \Delta \varphi_{sc,B1I}) \\ Q_{SCBOC,i} &= d \sqrt{2P_{B1I}} R_{B1I} (\tau - \hat{\tau}_c + \tau') \sin(\Delta \varphi + \Delta \varphi_{sc,B1I}). \end{aligned} \quad (14)$$

Considering that the E and L correlator results are used by the DLL as in standard GNSS receivers, detailed DLL operations are not discussed further. Similarly, the B1C prompt correlator results are utilized by the PLL as in standard GNSS receivers, so the PLL operations are not discussed further. The following discussion focuses on the operation of the SPLL.

From Equation (14), it is finally possible to design subcarrier discriminators to estimate the subcarrier parameters. In particular, two classes of SPLL discriminators can be employed. The first class is coherent discriminators, in

which the effect of the residual carrier phase is neglected ($\Delta\varphi = 0$) and the SPLL operates by assuming perfect carrier synchronization, while the other class is noncoherent discriminators, which are designed to operate even in the presence of the residual carrier phase errors ($\Delta\varphi \neq 0$). For the coherent discriminators, an example can be

$$\phi_{c,SCBOC}(\Delta\varphi_{sc,B1I}) = \arctan\left(\frac{Q_{SCBOC,P}}{I_{SCBOC,P}}\right) \quad (15)$$

when the residual carrier phase is small enough and can be approximated as $\Delta\varphi = 0$, the P correlator results can be directly used to calculate the subcarrier phase-estimation error. Note that other coherent discriminators used in standard PLLs can be similarly applied. For the noncoherent discriminators, an example can be

$$\begin{aligned} & \phi_{nc,SCBOC}(\Delta\varphi_{sc,B1I}) \\ &= \arctan\left(\frac{Q_{SCBOC,P}I_{B1C,P} + I_{SCBOC,P}Q_{B1C,P}}{I_{SCBOC,P}I_{B1C,P} - Q_{SCBOC,P}Q_{B1C,P}}\right). \end{aligned} \quad (16)$$

The working principle of Equation (16) can be verified by trigonometric identity. It clearly emerges that $\phi_{nc,SCBOC}$ is insensitive to residual carrier phase variations and equals $\Delta\varphi_{sc,B1I}$. After obtaining the subcarrier phase-estimation error $\Delta\varphi_{sc,B1I}$, the subcarrier dimension delay estimation $\hat{\tau}_s$ can be easily calculated by substituting $\Delta\varphi_{sc,B1I}$ into Equation (13) when the subcarrier frequency $f_{sc,B1I}$ is perfectly synchronized, which means $\hat{f}_{sc,B1I} \approx f_{sc,B1I}$.

The discriminator output is then filtered and a new estimate of the subcarrier frequency $\hat{f}_{sc,B1I}$ is produced by the numerically controlled oscillator (NCO). Note that the loop filter can be designed by using standard techniques. Additionally, similar to the standard PLLs, the subcarrier residual phase $\Delta\varphi_{sc,B1I}$ is driven to zero by adjusting the estimated subcarrier frequency $\hat{f}_{sc,B1I}$. The locally generated subcarrier can be obtained by subcarrier NCO using the new estimate of the subcarrier frequency, thus closing the subcarrier tracking loop.

When the unambiguous but low-precision code dimension delay estimation $\hat{\tau}_c$ from DLL and the high-precision but ambiguous subcarrier dimension delay estimation $\hat{\tau}_s$ from SPLL are obtained, the final propagation delay estimation can be represented as

$$\hat{\tau} = \hat{\tau}_s + \text{round}\left(\frac{\hat{\tau}_c - \hat{\tau}_s}{T_s}\right) \times T_s, \quad (17)$$

where $T_s = \frac{1}{2f_{sc,B1I}}$ is the subcarrier chip width.

As mentioned earlier, Figure 5 provides some optional optimization schemes, such as a carrier-aided code technique (Mower, 1991) and a subcarrier-aided code technique

(O'Driscoll, Avila-Rodriguez, & Ioannides, 2016). The corresponding aided coefficient can be calculated by

$$k_1 = \frac{f_c}{f_{B1}} \quad k_2 = \frac{f_c}{f_{sc,B1I}}, \quad (18)$$

where k_1 and k_2 are the aided coefficient of carrier- and subcarrier-aided code technique, respectively.

To sum up, such a CAT architecture fully utilizes the performance characteristics of each component in the B1 composite signal, i.e., the stable carrier estimation result of the B1C component and the high-precision delay estimation value of the B1I component. Considering the coherence between components in the composite signal, the phase-estimation result of the one signal component can be replaced by that of the other component. Therefore, the CAT technique cannot only perfectly track the complex correlation function but also greatly simplify the implementation complexity of the receiver.

5 | PERFORMANCE ANALYSIS

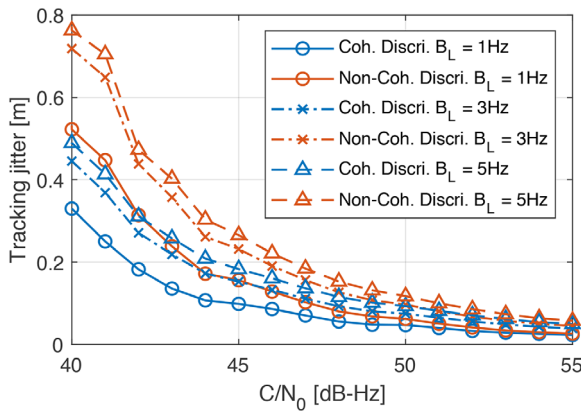
This section is mainly divided into two parts. The first uses a simulated signal to analyze the thermal noise performance of the CAT method. The second one uses the real signal data broadcast by BDS-3 satellites to verify the correctness and effectiveness of the proposed algorithm and further investigate the performance of the CAT technique.

5.1 | Simulation signal analysis

In this subsection, the thermal noise performance of the proposed CAT loop is analyzed using simulated BDS B1 wideband composite signals. It should be noted that the influence of the authorized service B1A signal and the additional intermodulation term on the open-service signal component receiving can be ignored due to the transparency characteristic of the CEMIC technique. Therefore, the simulated BDS B1 wideband composite signals can be generated as shown in open-service composite signal (5) instead of constant envelope composite signal (1). In addition, note that all the simulated signals are generated at the intermediate frequency (IF) level rather than radio frequency (RF) level to simplify processing complexity. Besides, the receiver front-end bandlimiting filter is not considered in the generation of the simulated signals. The simulation scenario is as follows: the real range is always kept constant. By introducing the Gaussian white noise of different power levels into simulated signals, the tracking jitter performance of the proposed CAT loop under thermal noise conditions, which is the standard deviation

TABLE 2 Parameters used in the simulation signal analysis

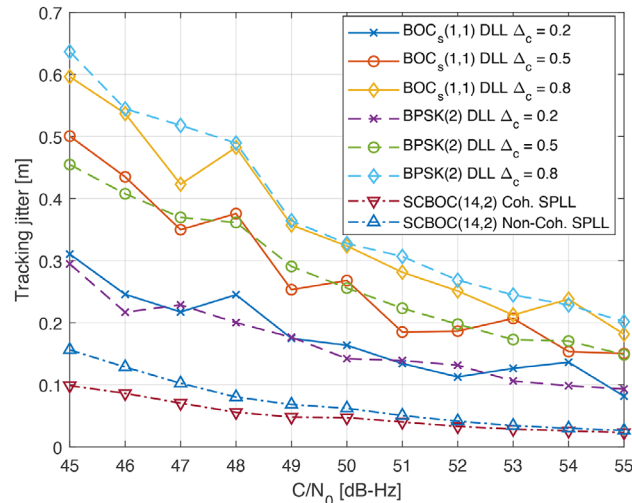
Parameter	Value
Sampling type	Complex I and Q
Sampling frequency	40 MHz
DLL order	2
DLL bandwidth	1 Hz
DLL early-minus-late spacing	0.2 chips/0.5 chips/0.8 chips
SPLL order	2
SPLL bandwidth	1 Hz/3Hz/5Hz
Integration time	1 ms

FIGURE 6 Tracking jitter of the SPLL with coherent and noncoherent discriminators for different loop bandwidths [Color figure can be viewed in the online issue, which is available at wileyonlinelibrary.com and www.ion.org]

of the pseudorange measurement, can be statistically obtained. For comparison, the thermal noise performance of a conventional GNSS receiver using other unambiguous methods for tracking and processing simulated composite signals is also given under the same conditions.

Table 2 shows the parameters used in the simulation signal analysis. The complex sampling is used, and the sampling frequency is 40 MHz, which is wide enough to contain the whole first main lobe of the SCBOC(14,2) modulated signal. The code loop is implemented using a second-order DLL with a loop bandwidth of 1 Hz, and different early-minus-late discriminator spacings are used to analyze the influence of discriminator spacing on tracking jitter. The subcarrier loop is implemented using a second-order PLL, and different loop bandwidths are used to analyze its effect on thermal noise performance. The coherent integration time is constant at 1 ms.

Figure 6 shows the tracking jitter of the SPLL with coherent and noncoherent discriminators for different loop bandwidths. The early-minus-late correlator spacing is $\Delta_c = 0.2$. In Figure 6, the tracking jitter is provided as a function of the input carrier-to-noise ratio $\frac{C}{N_0}$ and is expressed in units of meters. As can be seen from Figure 6,

FIGURE 7 Comparison of the tracking jitter performance of several unambiguous methods for tracking and processing B1I wideband composite signals with different early-minus-late correlator spacing [Color figure can be viewed in the online issue, which is available at wileyonlinelibrary.com and www.ion.org]

the tracking jitter of the SPLL increases as the loop bandwidth increases. In addition, comparing the results of the coherent and noncoherent discriminators, it can be found that the tracking jitter performance of the noncoherent discriminator is worse than that of the coherent discriminator due to the square loss. Also, it can be seen that the lower the $\frac{C}{N_0}$, the greater the influence of the square loss.

Figure 7 shows the comparison of the tracking jitter performance of several unambiguous methods for tracking and processing B1I wideband composite signals under conditions of different early-minus-late correlator spacing. What is marked with “SCBOC(14,2)” is the tracking jitter performance of the SPLL when the B1I component in the simulated composite signal is processed using the proposed CAT technology. The result of labeling “BPSK(2)” is the tracking jitter performance of the DLL when the BPSK-like unambiguous method (Martin et al., 2003) is used to process the B1I component in the simulated composite signal. The result of labeling “BOC(1,1)” is the tracking jitter performance of the DLL when the B1C pilot BOC(1,1) component in the simulated composite signal is processed using the Bump-Jumping unambiguous method (Fine & Fine, 1999). The loop bandwidth of both the DLL and the SPLL is 1 Hz. It can be seen from Figure 7 that the tracking jitter of the BPSK(2) and BOC(1,1) DLLs decreases as the discriminator spacing decreases. However, even if the BPSK(2) and BOC(1,1) DLLs choose a narrow correlator technique, that is, $\Delta_c = 0.2$, their thermal noise performance is still much worse than that of the SCBOC(14,2) SPLL. Therefore, it can be seen from the comparison results that the SCBOC(14,2) modulated signal does have



FIGURE 8 Working environment and workflow of the raw IF data recorder [Color figure can be viewed in the online issue, which is available at wileyonlinelibrary.com and www.ion.org]

great potential in ranging performance and the proposed CAT technique can fully exploit its ranging performance.

5.2 | Real data processing

In this subsection, the real signal data broadcast by BDS-3 satellites is used to verify the correctness and effectiveness of the proposed algorithm and further investigate the performance of the CAT technique. More specifically, a software receiver (Gao, Yao, & Lu, 2019) with configurable front end is used as the raw IF data recorder to collect real signals from BDS-3 satellites. A post-processing software receiver is developed for real data processing. It should be noted that the data-set used in this paper was collected on October 29, 2019, which contains valid B1 wideband composite signals since there are already 26 BDS-3 satellites in orbit.

Figure 8 shows the working environment and workflow of the raw IF data recorder. The full L-band antenna with a low noise amplifier (LNA) was laid on the roof of the

Weiqing Building of Tsinghua University in Beijing where the latitude and longitude coordinates are 40.001461 and 116.330074, respectively. First, the antenna receives all RF signals from visible satellites in the horizon. Second, the front-end downconverts the received RF signals to the IF signals. Third, the data acquisition module converts the analog IF signals into digital baseband signals, which are then stored in PC as raw IF data and then wait to be processed.

Table 3 shows the parameters used in adopting real IF signal data. The central frequency of the RF signal is 1575.42 MHz. The front-end filter bandwidth is 40 MHz. The complex sampling is used and the sampling frequency is 40 MHz. Therefore, zero-IF complex digital signals are obtained as raw IF data. It is not difficult to verify that the used parameters are justified from the conclusions in Section 3.

Table 4 shows the parameters used in the receiver for real data processing. The carrier loop is achieved using a second-order frequency lock loop (FLL) aided three-order PLL. The code loop is implemented using a second-order

TABLE 3 Parameters used in adopting real IF signal data

Parameter	Value
RF central frequency	1575.42 MHz
Front-end filter bandwidth	40 MHz
IF central frequency	0 Hz
Sampling frequency	40 MHz
Sampling type	Complex I and Q
No. of bits	16
Date	29 October 2019

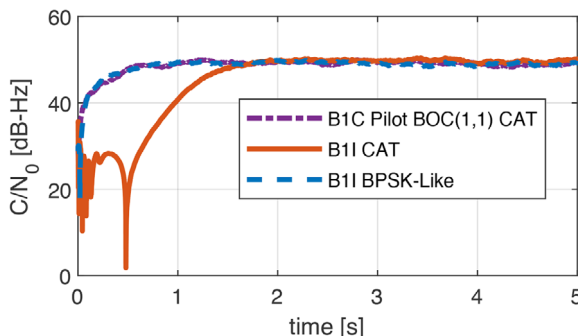
TABLE 4 Parameters used in the receiver for real data processing

Parameter	Value
FLL order	2
FLL bandwidth	2 Hz
PLL order	3
PLL bandwidth	20 Hz
DLL order	2
DLL bandwidth	5 Hz
DLL early-minus-late spacing	0.2 chips
SPLL order	2
SPLL bandwidth	5 Hz
Integration time	1 ms

DLL, and the subcarrier loop is implemented using a second-order PLL. The coherent integration time is still constant at 1 ms, which is the length of one code period. It should be noted that the loop parameters used are typical values for land applications.

The real data processing results mainly include four aspects: $\frac{C}{N_0}$ estimation, correlator output results, correlation curve, and single-point positioning results.

Figure 9 shows the results of the $\frac{C}{N_0}$ estimation for the B1 wideband composite signal, including the results of

**FIGURE 9** $\frac{C}{N_0}$ estimation for the B1 wideband composite signal [Color figure can be viewed in the online issue, which is available at wileyonlinelibrary.com and www.ion.org]

the B1C pilot BOC(1,1) component, and the results of the SCBOC(14,2) modulated signal using the proposed CAT technique and a BPSK-like method. It can be seen from Figure 9 that after about 2 seconds, the $\frac{C}{N_0}$ of the proposed method tends to be stable, which means the CAT technique can stably track the SCBOC(14,2) modulated signal. Compared with the BPSK-like tracking method, the CAT technique takes a longer time to enter the stable tracking phase, which is because the carrier needs to be tracked stably at first and then the complex subcarrier starts to effectively demodulate.

Figure 10 shows the correlator output results of the CAT technique for the B1 composite signal. Figure 10a is the prompt correlator output of the B1C pilot BOC(1,1) component, including the in-phase (I) and quadrature (Q) parts. Comparing the amplitudes of the I and Q parts, it can be clearly seen that the main energy of the prompt correlator output is maintained in the I branch rather than the Q branch, which means the carrier of the composite signal has been perfectly tracked. In addition, it can be seen that the overlay code modulated on the B1C pilot component is also parsed in the in-phase branch.

Figure 10b is the prompt correlator output of the SCBOC(14,2) component, including the I and Q parts. Similarly, it can be seen that the main energy of the prompt correlator output is retained in the I branch and the BII navigation message can be clearly demodulated.

Figure 10c is the E, P, L correlator output in code dimension of the SCBOC(14,2) modulated signal. It can be seen that the P correlator output is always greater than the E and L correlator output, which means the code dimension of the SCBOC(14,2) modulated signal can be well-tracked.

Figure 10d is the prompt correlator output in subcarrier dimension of the SCBOC(14,2) modulated signal, including the I and Q parts. It can be seen that the main energy of the subcarrier dimension is always maintained in the I branch, which means the single-sideband complex subcarrier of the SCBOC(14,2) modulated signal can also be perfectly estimated. These correlator output results indicate that the proposed CAT algorithm can achieve stable matching reception of the B1 wideband composite signal.

Using multiple sets of correlators, Figure 11 shows the correlation function curve of the B1 composite signal, including the real part, the imaginary part, and the amplitude of the correlation function. Figure 11a is the code dimension correlation curve of the SCBOC(14,2) modulated signal using the CAT technique, that is, $\hat{\tau}_s = \tau$. It can be seen that code dimension correlation curve is a typical ACF of the BPSK modulated signal and the delay estimation from code dimension is unambiguous but low-precision.

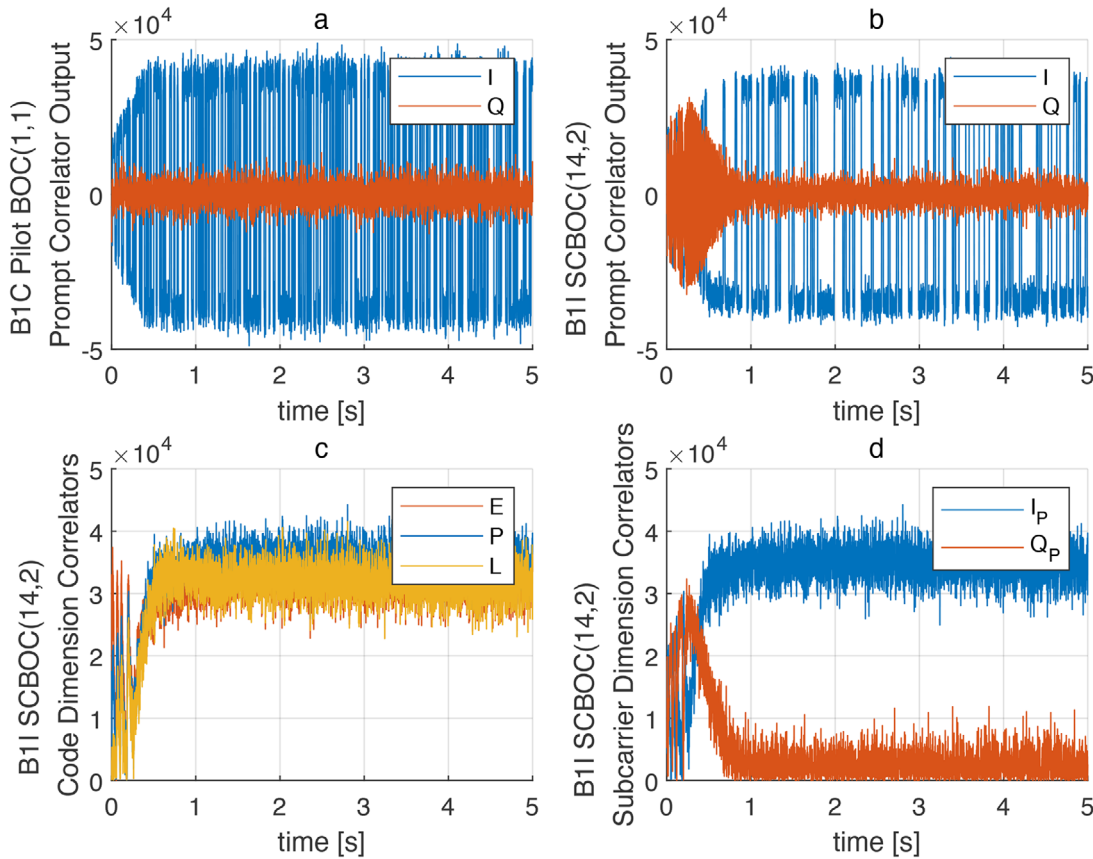


FIGURE 10 Correlator output results of the CAT technique [Color figure can be viewed in the online issue, which is available at wileyonlinelibrary.com and www.ion.org]

Figure 11b is the subcarrier-dimension correlation curve of the SCBOC(14,2) modulated signal using the CAT technique, that is, $\hat{\tau}_c = \tau$. It can be seen that subcarrier-dimension correlation curve is a periodic complex function. Since the subcarrier frequency is high relative to the code rate, the delay estimation from subcarrier dimension is ambiguous but high-precision.

Figure 11c is the composite dimension correlation curve of the SCBOC(14,2) modulated signal using the CAT technique, that is, $\hat{\tau}_c = \hat{\tau}_s$. It can be seen that the composite correlation curve is a complex function, which matches the theoretical ACF in Figure 4 well.

Figure 11d also gives the correlation function curve of the B1C pilot BOC(1,1) component. It can be seen that it also agrees well with the theoretical ACF of BOC(1,1) modulated signal. Therefore, the monitoring results of the correlation function curve show that the proposed CAT technique can achieve high-performance stable tracking for the B1 composite signal.

The above results show the measurement performance of a single channel using the CAT technique, and the following parts analyze the positioning performance of the proposed method. The experimental time was selected at 12:32 on October 29, 2019, Beijing time. Figure 12 shows

the skyplot of the BDS-3 at that time. It should be noted that only the available satellites that simultaneously broadcast the B1C and B1I signals are considered here. It can be seen from Figure 12 that there are six available BDS-3 satellites, and their PRN numbers are 21, 26, 28, 33, 34, and 38, respectively. The position dilution of precision (PDOP) value is 2.24, which is enough to complete stable single-point positioning.

Figure 13 shows the comparison of the horizontal positioning errors using CAT and BPSK-like techniques for the SCBOC(14,2) modulated signal. It can be clearly seen from Figure 13 that the proposed CAT technique has a significant positioning precision improvement due to the utilization of the high-frequency subcarrier ranging performance. In this experiment, although only 6 satellites are available, which means the PDOP value has room for improvement when the BDS-3 reaches full operational capability (FOC), the horizontal positioning error using the CAT technique is still small. More specifically, compared with the traditional BPSK-like reception mode, the CAT method reduces the east error from about ± 4 m to ± 0.5 m, and the north error is reduced from around ± 6 m to ± 1 m. It is not difficult to predict that when the number of available satellites increases, the distribution

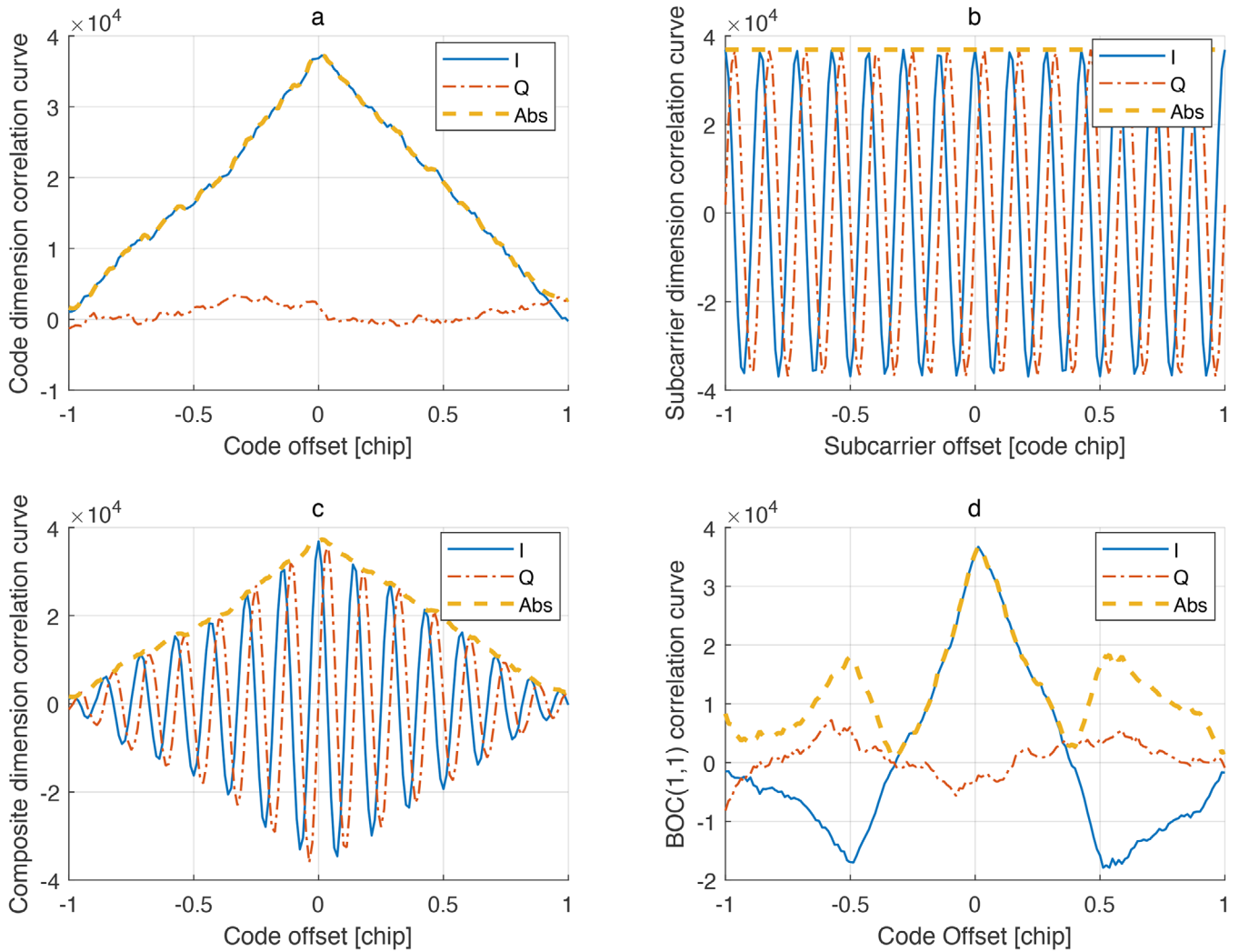


FIGURE 11 Correlation function curve of the B1 composite signal [Color figure can be viewed in the online issue, which is available at wileyonlinelibrary.com and www.ion.org]

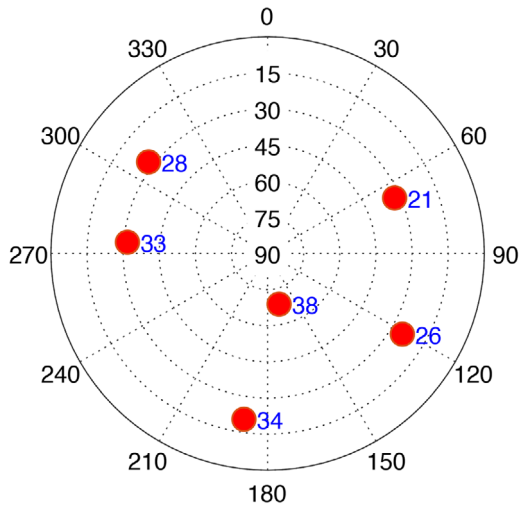


FIGURE 12 Skyplot of the dataset [Color figure can be viewed in the online issue, which is available at wileyonlinelibrary.com and www.ion.org]

of visible satellites can be improved. At that time, the positioning performance using the CAT algorithm can be further improved, perhaps even to submeter positioning applications.

These results verify the correctness and effectiveness of the proposed algorithm. The experimental results show that the CAT algorithm can achieve better ranging performance and higher positioning precision. In the future, the other performance parameters of the CAT technique, such as tracking sensitivity, anti-multipath performance and so on, should be further analyzed.

6 | CONCLUSIONS AND FUTURE WORK

This paper proposes an unambiguous CAT method based on two-dimensional loops for the BDS B1 wideband composite signal. The CAT technique makes full use of the

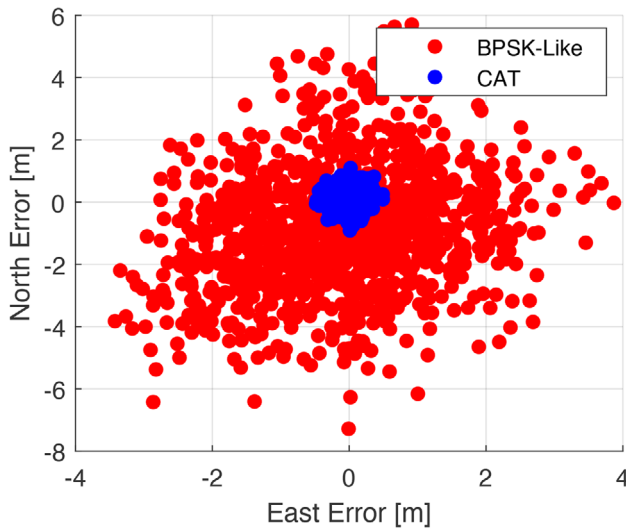


FIGURE 13 The comparison of the horizontal positioning errors using CAT and BPSK-like technique [Color figure can be viewed in the online issue, which is available at wileyonlinelibrary.com and www.ion.org]

coherence and signal structure of the composite signal to obtain high-precision ranging and positioning performance. The experimental results verify the correctness and effectiveness of the proposed algorithm. More specifically, the work and contribution of this paper mainly include three aspects.

First, the receiving mode for obtaining high-precision ranging and positioning performance using the single-sideband complex subcarrier modulation, which is introduced for backward compatibility in the BDS-3 B1 wideband composite signal, is proposed for the first time. In order to meet the constraints of a smooth evolutionary transition and backward compatibility of the BDS, a unique SCBOC(14,2) subcarrier is adopted in the B1 band in BDS-3 to construct a composite signal. The characteristics of the new SCBOC(14,2) modulated signal, including PSD, ACF, and Gabor bandwidth, are analyzed. The results show that the SCBOC(14,2) modulated signal has great potential for improving ranging performance.

Second, a specific implementation method of the B1 wideband composite signal high-precision tracking is proposed. More specifically, an unambiguous CAT method based on two-dimensional loops is proposed. The inherent coherence between the components in the composite signal is used to solve the problem that the complex correlation function cannot be tracked. The 2-D loop structure is used to transform the signal correlation function into a 2-D space to solve the tracking ambiguity threat. In addition, several optional optimization schemes are provided to improve receiver performance.

Third, simulated signal analysis and real BDS-3 signal processing are carried out for performance analysis of the CAT technique. The results verify the correctness and effectiveness of the proposed algorithm. In addition, the results show that compared to the traditional tracking processing for independent components, the proposed CAT technique for the composite signal can significantly improve ranging precision, leading to a higher positioning precision.

In general, this paper pioneers a high-precision processing mode for the BDS-3 B1 composite signal, which can provide a great reference and guidance for high-precision utilization of the new generation BDS signals. As for future work, the theoretical performance analysis of the proposed method, including thermal noise and multipath performance, should be studied. In addition, the influence of the DLL correlator spacing on the SPLL thermal noise performance when using the proposed CAT technique and its optimal parameter selection rule also should be investigated. Meanwhile, the performance of the proposed method under the complex environment or weak signal conditions also should be paid attention to.

ACKNOWLEDGEMENT

This work was supported by the National Natural Science Foundation of China (Grant No. 61771272). The recorded raw IF data used in Section 5.2 has been uploaded to the net disk and can be downloaded by the link: <https://cloud.tsinghua.edu.cn/d/b1720900deca452dad66/>.

ORCID

Yang Gao  <https://orcid.org/0000-0002-2177-5804>
Zheng Yao  <https://orcid.org/0000-0002-7657-644X>

REFERENCES

- Betz, J. W. (2001). Binary offset carrier modulations for radionavigation. *NAVIGATION*, 48(4), 227–246. <https://doi.org/10.1002/j.2161-4296.2001.tb00247.x>
- Borio, D. (2014). Double phase estimator: New unambiguous binary offset carrier tracking algorithm. *IET Radar Sonar and Navigation*, 8(7), 729–741. <https://doi.org/10.1049/iet-rsn.2013.0306>
- Borio, D. (2017). Coherent side-band BOC processing. *IET Radar, Sonar & Navigation*, 11(10), 1455–1466. <https://doi.org/10.1049/iet-rsn.2016.0245>
- Fine, P., & Fine, W. (1999). Tracking algorithm for GPS offset carrier signals. In *Proceedings of the 1999 National Technical Meeting of The Institute of Navigation*, pp. 671–676. Retrieved from <https://www.ion.org/publications/abstract.cfm?articleID=719>
- Gao, Y., Yao, Z., & Lu, M. (2018). Theoretical analysis of unambiguous 2-D tracking loop performance for band-limited BOC signals. *GPS Solutions*, 22(1), 30. <https://doi.org/10.1007/s10291-017-0695-5>
- Gao, Y., Yao, Z., & Lu, M. (2019). Design and implementation of a real-time software receiver for BDS-3 signals. *NAVIGATION*, 66(1), 83–97. <https://doi.org/10.1002/navi.290>

- Hein, G. W., Avila-Rodriguez, J.-A., Wallner, S., Pratt, A. R., Owen, J., Issler, J., ... Stansell, T. A. (2006). MBOC: The new optimized spreading modulation recommended for GALILEO L1 OS and GPS L1C. In *Proceedings of IEEE/ION PLANS 2006*, pp. 883–892. <https://doi.org/10.1109/PLANS.2006.1650688>
- Hodgart, M. S., Blunt, P.D., & Unwin, M. (2007). The optimal dual estimate solution for robust tracking of binary offset carrier (BOC) modulation. In *Proceedings of the 20th International Technical Meeting of the Satellite Division of The Institute of Navigation (ION GNSS 2007)*, pp. 1017–1027. Retrieved from <https://www.ion.org/publications/abstract.cfm?articleID=7604>
- Julien, O., Macabiau, C., Cannon, M. E., & Lachapelle, G. (2007). ASPeCT: Unambiguous sine-BOC(n,n) acquisition/tracking technique for navigation applications. *IEEE Transactions on Aerospace & Electronic Systems*, 43(1), 150–62. <https://doi.org/10.1109/TAES.2007.357123>
- Lestarquit, L., Artaud, G., & Issler, J.-L. (2008). AltBOC for dummies or everything you always wanted to know about AltBOC. In *Proceedings of the 21st International Technical Meeting of the Satellite Division of The Institute of Navigation (ION GNSS 2008)*, pp. 961–970. Retrieved from <https://www.ion.org/publications/abstract.cfm?articleID=8018>
- Lohan, E. S., & Borre, K. (2016). Accuracy limits in multi-GNSS. *IEEE Transactions on Aerospace and Electronic Systems*, 52(5):2477–2494. <https://doi.org/10.1109/TAES.2016.150241>
- Lohan, E. S., de Diego, D. A., Lopez-Salcedo, J. A., Seco-Granados, G., Boto, P., & Fernandes, P. (2017). Unambiguous techniques modernized GNSS signals: Surveying the solutions. *IEEE Signal Processing Magazine*, 34(5), 38–52. <https://doi.org/10.1109/MSP.2017.271778>
- Lohan, E. S., Lakhzouri, A., & Renfors, M. (2006). Complex double-binary-offset-carrier modulation for a unitary characterisation of Galileo and GPS signals. *IEEE Proceedings-Radar, Sonar and Navigation*, 153(5), 403–408. <https://doi.org/10.1049/ip-rsn:20060005>
- Martin, N., Leblond, V., Guillotel, G., & Heiries, V. (2003). BOC(x,y) signal acquisition techniques and performances. In *Proceedings of the 16th International Technical Meeting of the Satellite Division of The Institute of Navigation (ION GPS/GNSS 2003)*, pp. 188–198. Retrieved from <https://www.ion.org/publications/abstract.cfm?articleID=5194>
- Mower, V. L. (1991). U.S. Patent No. 5,003,552A. Washington, DC: U.S. Patent and Trademark Office.
- O'Driscoll, C., Ávila-Rodríguez, J., & Ioannides, R. (2016). Subcarrier aided code tracking of high order BOC signals. In *Proceedings of the 29th International Technical Meeting of the Satellite Division of The Institute of Navigation (ION GNSS+ 2016)*, pp. 444–458. <https://doi.org/10.33012/2016.14837>
- Ren, J., Jia, W., Chen, H., & Yao, M. (2012). Unambiguous tracking method for alternative binary offset carrier modulated signals based on dual estimate loop. *IEEE Communications Letters*, 16(11), 1737–1740. <https://doi.org/10.1109/LCOMM.2012.092112.121853>
- Schubert, F. M., Wendel, J., Soellner, M., Kaindl, M., & Kohl, R. (2014). The astrium correlator: Unambiguous tracking of high-rate boc signals. In *IEEE-ION Position Location and Navigation Symposium 2014*, pp. 589–601. <https://doi.org/10.1109/PLANS.2014.6851420>
- Sleewaegen, J.-M., De Wilde, W., & Hollreiser, M. (2004). Galileo AltBOC receiver. In *Proceedings of European Navigation Conference GNSS 2004*. Retrieved from <https://www.septentrio.com/sites/default/files/2019-12/Septentrio-Paper-2014-Sleewaegen-De-Wilde-Galileo-AltBOC-GNSS-Receiver.pdf>
- Tian, F., Zhang, K., & Cheng, L. (2016). Unambiguous tracking of BOC signals using coherent combination of dual sidebands. *IEEE Communications Letters*, 20(8), 1555–1558. <https://doi.org/10.1109/LCOMM.2016.2569520>
- Ward, P. W. (2003). A design technique to remove the correlation ambiguity in binary offset carrier (BOC) spread spectrum signals. In *Proceedings of the 59th Annual Meeting of The Institute of Navigation and CIGTF 22nd Guidance Test Symposium*, pp. 146–155. Retrieved from <https://www.ion.org/publications/abstract.cfm?articleID=3844>
- Yao, Z., Cui, X., Lu, M., & Feng, Z. (2010). Pseudo-correlation-function-based unambiguous tracking technique for sine-BOC signals. *IEEE Transactions on Aerospace & Electronic Systems*, 46(4), 1782–1796. <https://doi.org/10.1109/TAES.2010.5595594>
- Yao, Z., Gao, Y., Gao, Y., & Lu, M. (2017). Generalized theory of BOC signal unambiguous tracking with two-dimensional loops. *IEEE Transactions on Aerospace and Electronic Systems*, 53(6), 3056–3069. <https://doi.org/10.1109/TAES.2017.2726878>
- Yao, Z., Guo, F., Ma, J., & Lu, M. (2017). Orthogonality-based generalized multicarrier constant envelope multiplexing for DSSS signals. *IEEE Transactions on Aerospace and Electronic Systems*, 53(4), 1685–1698. <https://doi.org/10.1109/TAES.2017.2671580>
- Yao, Z., & Lu, M. (2013). Constant envelope combination for components on different carrier frequencies with unequal power allocation. In *Proceedings of the 2013 International Technical Meeting of The Institute of Navigation*, pp. 629–637. Retrieved from <https://www.ion.org/publications/abstract.cfm?articleID=10838>
- Yao, Z., & Lu, M. (2017). Signal multiplexing techniques for GNSS: The principle, progress, and challenges within a uniform framework. *IEEE Signal Processing Magazine*, 34(5), 16–26. <https://doi.org/10.1109/MSP.2017.2713882>
- Yao, Z., Zhang, J., & Lu, M. (2016). ACE-BOC: Dual-frequency constant envelope multiplexing for satellite navigation. *IEEE Transactions on Aerospace and Electronic Systems*, 52(1), 466–485. <https://doi.org/10.1109/TAES.2015.140607>
- Zhou, H., Yao, Z., & Lu, M. (2016). A quasi-coherent receiving algorithm and its performance verification for composite signals of next generation GNSS. In *Proceedings of the 2016 International Technical Meeting of The Institute of Navigation*, pp. 591–599. <https://doi.org/10.33012/2016.13438>
- Zhu, Y., Cui, X., & Lu, M. (2015). Dual binary phase-shift keying tracking method for Galileo E5 AltBOC (15, 10) signal and its thermal noise performance. *IET Radar, Sonar & Navigation*, 9(6), 669–680. <https://doi.org/10.1049/iet-rsn.2014.0349>

How to cite this article: Gao Y, Yao Z, Lu M. High-precision unambiguous tracking technique for BDS B1 wideband composite signal. *NAVIGATION*. 2020;67:633–650. <https://doi.org/10.1002/navi.377>

APPENDIX: THE PSD DERIVATION OF THE SCBOC(14,2) MODULATED SIGNAL

In this Appendix, we present the detailed PSD derivation of the SCBOC(14,2) modulated signal using the methods in Lohan's paper (Lohan, Lakhzouri, & Renfors, 2006, Lohan & Borre, 2016).

The baseband complex envelope of the SCBOC(14,2) modulated signal can be represented as

$$\begin{aligned} s_{SCBOC}(t) = & D_{B1I}(t) C_{B1I}(t) \left(\text{sign}(\cos(2\pi f_{sc,B1I} t)) \right. \\ & \left. - j \cdot \text{sign}(\sin(2\pi f_{sc,B1I} t)) \right). \end{aligned} \quad (19)$$

Figure 14 shows the block diagram of the baseband modulation of the SCBOC(14,2) modulated signal.

Using the conclusions from Lohan's paper, the PSD of all GNSS signals can be uniformly described by the frequency domain equivalent transfer function. Figure 15 shows the block diagram of the frequency domain equivalent transfer function of the SCBOC(14,2) modulated signal.

Therefore, the frequency domain equivalent transfer function of the SCBOC(14,2) modulated signal $M_{SCBOC}(f)$ can be represented as

$$\begin{aligned} M_{SCBOC}(f) = & R_{28}(f) C_{14}(f) \\ & - j R_{28}(f) S_{14}(f) H_{28 \rightarrow 14}(f), \end{aligned} \quad (20)$$

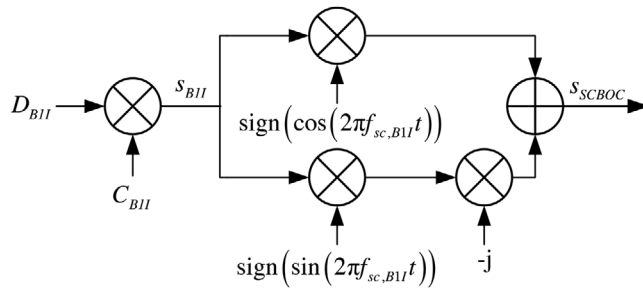


FIGURE 14 The block diagram of the baseband modulation of the SCBOC(14,2) modulated signal

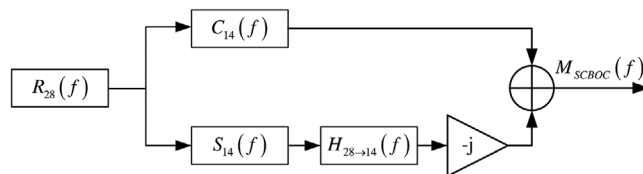


FIGURE 15 The block diagram of the frequency domain equivalent transfer function of the SCBOC(14,2) modulated signal

where $R_{N_1}(f)$, which is the Fourier transform of a rectangular pulse of width $\frac{T_c}{N_1}$ and called the rectangular transfer function of order N_1 , can be expressed as

$$R_{N_1}(f) = \frac{\sin\left(\pi f \frac{T_c}{N_1}\right)}{\pi f} \exp\left(-j\pi f \frac{T_c}{N_1}\right). \quad (21)$$

$S_N(f)$, which is the sine-BOC transfer function of modulation order N , can be defined as

$$S_N(f) = \frac{1 - (-1)^N \exp(-j2\pi f T_c)}{1 + \exp(-j2\pi f \frac{T_c}{N})}. \quad (22)$$

$C_N(f)$, which is the sine-BOC transfer function of modulation order N , can be defined as

$$C_N(f) = \frac{\left[\left(1 - (-1)^N \exp(-j2\pi f T_c) \right) \times \left(1 - (-1)^N \exp(-j2\pi f \frac{T_c}{N}) \right) \right]}{\left(1 + \exp(-j2\pi f \frac{T_c}{N}) \right) \left(1 + \exp(-j2\pi f \frac{T_c}{2N}) \right)}. \quad (23)$$

$H_{N_1 \rightarrow N}(f)$, which is the hold transfer function of a hold block that converts a signal of rate $N_1 f_0$ into a signal of rate $N f_0$ with $N_1 > N$, can be expressed as

$$H_{N_1 \rightarrow N}(f) = \frac{1 - \exp(-j2\pi f \frac{T_c}{N})}{1 - \exp(-j2\pi f \frac{T_c}{N_1})}. \quad (24)$$

Therefore, the PSD of the SCBOC(14,2) modulated signal can be given by

$$S_{SCBOC}(f) = \frac{1}{T_c} S_D(f) |M_{SCBOC}(f)|^2, \quad (25)$$

where $S_D(f)$ is the PSD of the modulated navigation data. Although, the PSD of the SCBOC(14,2) modulated signal will be affected by the PSD of the modulated navigation data. However, under the simplifying assumption that the navigation messages are built of zero-mean and uncorrelated chips, $S_D(f)$ is constant and equal to the sequence power, which equals 1. Substituting Equations (20)-(24) into Equation (25), after simplification, one can obtain the PSD of the SCBOC(14,2) modulated signal, which is in Equation (7).